2018

Impact of Suction and Injection Gas Superheat Degrees on The Performance of a Residential Heat Pump With Vapor Injection and Variable Speed Scroll Compressor

Bertrand Dechesne
University of Liège, Belgium, bdechesne@uliege.be

Lemort Vincent
University of Liege, Belgium, vincent.lemort@uliege.be

Madiha Nadri
Université Claude Bernard Lyon 1, madiha.nadri-wolf@univ-lyon1.fr

Pascal Dufour
Université Claude Bernard Lyon 1, pascal.dufour@univ-lyon1.fr

Impact of suction and injection gas superheat degrees on the performance of a residential heat pump with vapor injection and variable speed scroll compressor

Bertrand DECHESNE[1]*, Vincent Lemort[1], Madiha NADRI[2], Pascal DUFOUR[2]

[1]University of Liège, Aerospace & Mechanical engineering Dpt., Thermodynamics Laboratory
Liège, Belgium
bdechesne@uliege.be, vincent.lemort@uliege.be

[2] Université de Lyon, Université Claude Bernard Lyon 1, CNRS UMR 5007 LAGEP, 43 Boulevard du 11 Novembre 1918, 69100 Villeurbanne, France
madiha.nadri-wolf@univ-lyon1.fr, pascal.dufour@univ-lyon1.fr

* Corresponding Author

ABSTRACT

The first part of this paper focuses on the experimental results collected from a vapor injection and variable speed scroll compressor air-to-water residential heat pump. The unit is a 10 kW residential system working with R410a and capable of providing floor heating and domestic hot water. It is tested in a controlled environment in order to achieve a wide range of outdoor and indoor conditions. The impact on the system performance of the vapor superheat degrees at both injection and suction ports is discussed. It is shown that a better control of these variables could improve the system COP and heating capacity by respectively 10 and 15%. It is also shown that the control of the superheat degrees is a coupled problem and the use of standard gain-scheduled (Single Input Single Output) SISO proportional–integral–derivative (PID) controllers is not optimal.

The second part of this paper presents a multivariable decoupler-based proportional–integral (PI) controller using feedforward action in order to take into account the coupling between both superheat controls. System models are first presented, the first one is a MIMO (Multiple Input Multiple Output) first order transfer function based model in order to identify the decoupler and PI controller gains. The second one is a non-linear dynamic model of the injection line in order to first test the proposed controller in simulation. Finite-volume models are used for the heat exchangers and the split lines. A thermodynamic model of the vapor injection scroll compressor is developed using empirical correlations for the volumetric efficiency, isentropic efficiency and the ratio between the injection and suction mass flow rates. Three adapted multivariable controllers are tested in simulation and compared to a baseline PI controller. All proposed controllers show increased performances compared to the SISO PI controller.

1. INTRODUCTION

Nowadays, it is commonly accepted that our society has to take decisions and actions in order to minimize our impact on the environment and the climate. Among all of those taken in the last decades, the EU voted the 2020 legislation package that provides climate and energy targets by the 2020 horizon. One of these targets is a 20% improvement in energy efficiency and the heating and cooling sector has a major role to play.

In the field of vapor compression cycle (VCC), recent publications presented advances in these systems that are aiming at, somehow, an energy efficiency and performance improvement. Park *et al.* (2015) compared different advanced VCC architectures in order to identify the best potential for performance improvement. Taking into account the best efficiency they could find in the literature for each component, they showed that injection cycles are one the most promising technology in term of performance enhancement. In this field, Xu *et al.* (2011) gave a deep literature review comparing the different injection options and focusing both on the system level and the components level. Heo *et al.* (2011) compared different architectures of injection cycle and although the economizer architecture does not show the best performances, it has the advantage to be easier to control than the flash tank architecture

This paper aims at showing the impact of suction and injection gas superheat degrees on the performance of an injection heat pump with an economizer and variable speed scroll compressor. The coupling of the control of both expansion valve is also investigated. An adapted controller is then proposed for the injection line superheat control. This multivariable controller uses a feedforward action (decoupler) in order to improve the injection superheat control.

2. EXPERIMENTAL INVESTIGATIONS

In this section, the test rig is first presented and the impact of the levels of superheat on the system performance is discussed.

2.1 Set-up

The test-bench is schematized in Figure 1.

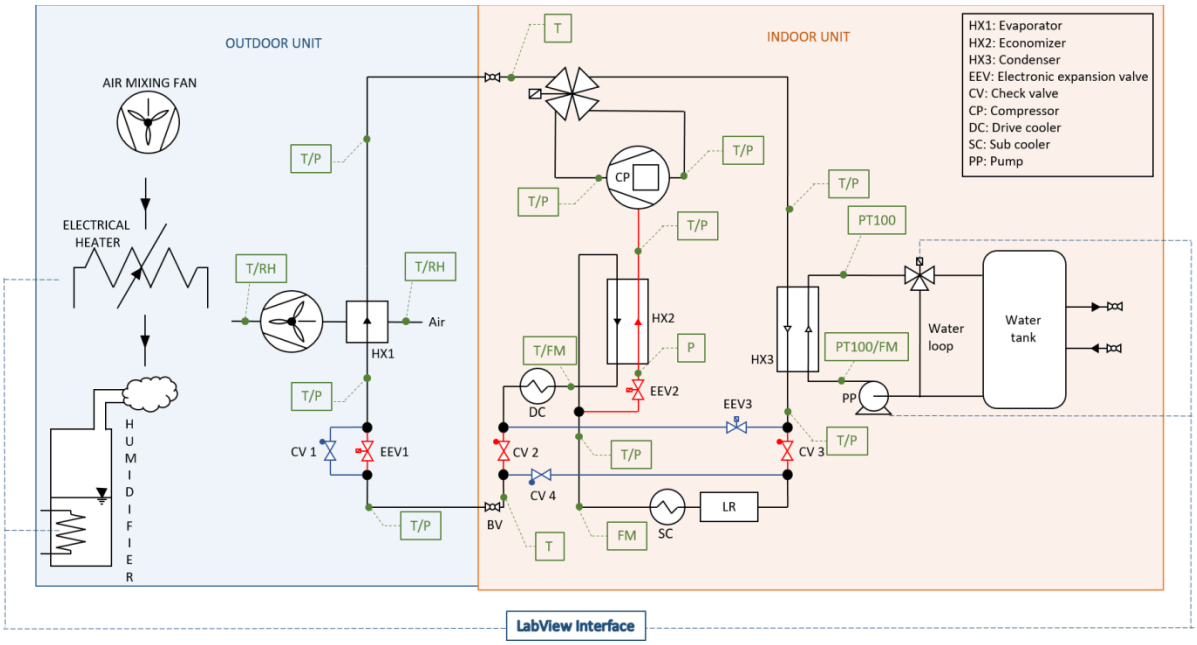

Figure 1: Experimental set-up scheme.

The refrigerant loop is controlled by means of a ModBus Interface, which implies the adjustment of the rotational speed of the air evaporator fan, of the scroll compressor, the openings of the electronic expansion valves (EEV) as well as the four-way valve. An additional heat exchanger, called drive cooler, is installed to cool down the power electronic used for the variation of the compressor speed.

Conditions in terms of temperature and absolute pressure are measured at the supply/exhaust of each component of the refrigerant loop. Temperatures are determined by means of sensor pockets (type T thermocouple) with accuracy of ±0.3 K. Used absolute pressure sensors show the following characteristics:

- Operating range of 0-20 bar for the sensor used at the supply of the compressor with an accuracy of 1% of the full scale range;
- Operating range of 0-30 bar for sensors used for measuring the low and intermediate pressure level with an accuracy of ±1% of the full scale range;
- Operating range of 0-50 bar for sensors used for measuring the high pressure with an accuracy of ±0.5% of the full-scale range.

The water flow passing through the condenser is controlled by adjusting the rotational speed of the water pump. The water temperature at the supply of the condenser can be controlled using a valve and tap water. Given the low temperature difference between the supply and the exhaust of the condenser (between 3 and 10K), PT100 with

accuracy of ±0.1 K have been preferred instead of type T thermocouple. Water flow rate is determined by means of an impulse water meter (4 pulses per liter). Table 1 gives the sensors and their respective accuracy.

Table 1: List of sensors and related accuracy.

Sensors	Error
Type T thermocouples	±0.3 K
PT100 class 1/10 DIN	±0.1 K
Keller 0-20 bar absolute pressure	±0.2 bar
Keller 0-30 bar absolute pressure	±0.3 bar
Keller 0-50 bar absolute pressure	±0.25 bar
Siemens SITRANS differential pressure	±0.05 mbar
Krohne Optimass 6000	±0.1 %
Emerson micro-motion CMF025	±0.1 %
Impulse water meter	4 pulses per liter
Power meter	±0.5 %

The outdoor unit is installed in a room where conditions are controlled in terms of both humidity and temperature. Relative humidity is controlled by the use of electrical steam generators (humidifier). It is also possible to control with precision the outdoor air temperature by means of a set of variable electrical resistances. The relative humidity at the inlet and at the outlet of the outdoor air stream passing through the air evaporator are measured by means of relative humidity sensors with an accuracy of ± 1.5 percent points.

2.2 Impact of superheat on system performance

Tests were carried out at constant speed and steady working conditions in order to investigate the impact of the superheat levels on the system performances. Results for a compressor rotational speed of 3000 RPM, an outside temperature of 0°C and a water inlet temperature of 55°C are presented in Figure 2. First of all, at time t=0, it can be seen that the superheat level at the exhaust of the evaporator and the suction port of the compressor is quite different. This is mainly due to the heat transfer in the four-way valve and, to a lower extend, the pressure drop in the vapor split line.

In phase I (time $\in$ [0; 1500[seconds), the outdoor electronic expansion valve (OEEV) opening is increased in order to reduce the superheat at the exhaust of the evaporator down to 5K. The coupled problem of superheat control is shown during this phase. In fact, the injection superheat increases during this phase even though the injection electronic expansion valve (IEEV) opening has remained constant. This is due to a higher mass flow rate on the high pressure side of the economizer because of the increased outdoor valve opening. At the end of phase I, the COP has increased from 2.25 to 2.54 while the heating capacity has increased by 16%. On the other end, the discharge temperature dropped from 115.3 to 110.3°C. These values have been averaged over 300 seconds.

In a second phase (time $\in$ [1500; 2500] seconds), the injection expansion valve opening is increased in order to bring the level of superheat back to 5K. It can be seen that no coupling occurs this time, i.e., the control of the injection expansion valve does not affect significantly the outdoor level of superheat. Decreasing the level of superheat on the injection line increase the amount of injected refrigerant and helps to increase by 3 additional percent the heating capacity compared to the end of phase I. The discharge temperature is also decreased to 102.9°C but the COP remains approximately constant compared to the end of previous phase (2.56). As a conclusion, in term of superheat control, it can be stated that the system has two inputs (both expansion valves openings) and two outputs (suction and injection superheats) with one of the non-diagonal element of the transfer matrix that is equal to zero (c.f. section 3.1).

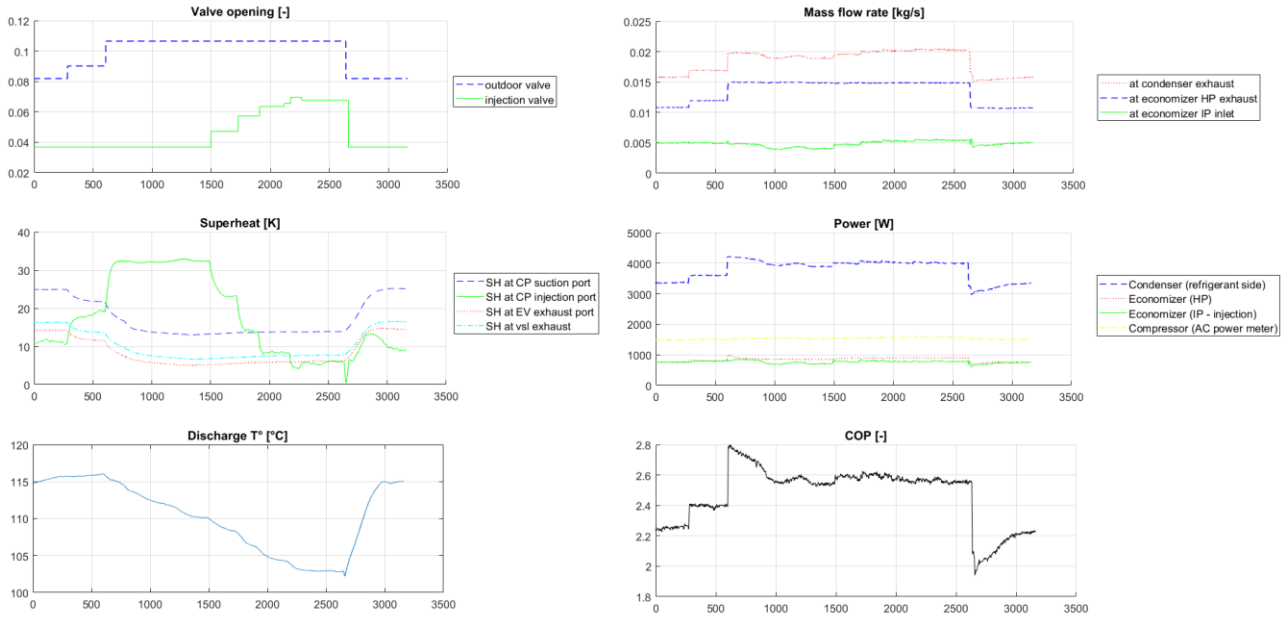

Figure 2: Experimental results for superheat analysis at constant working conditions as a function of time [s] (3000 RPM compressor speed, 0°C outdoor temperature and 50°C water supply temperature to the condenser).

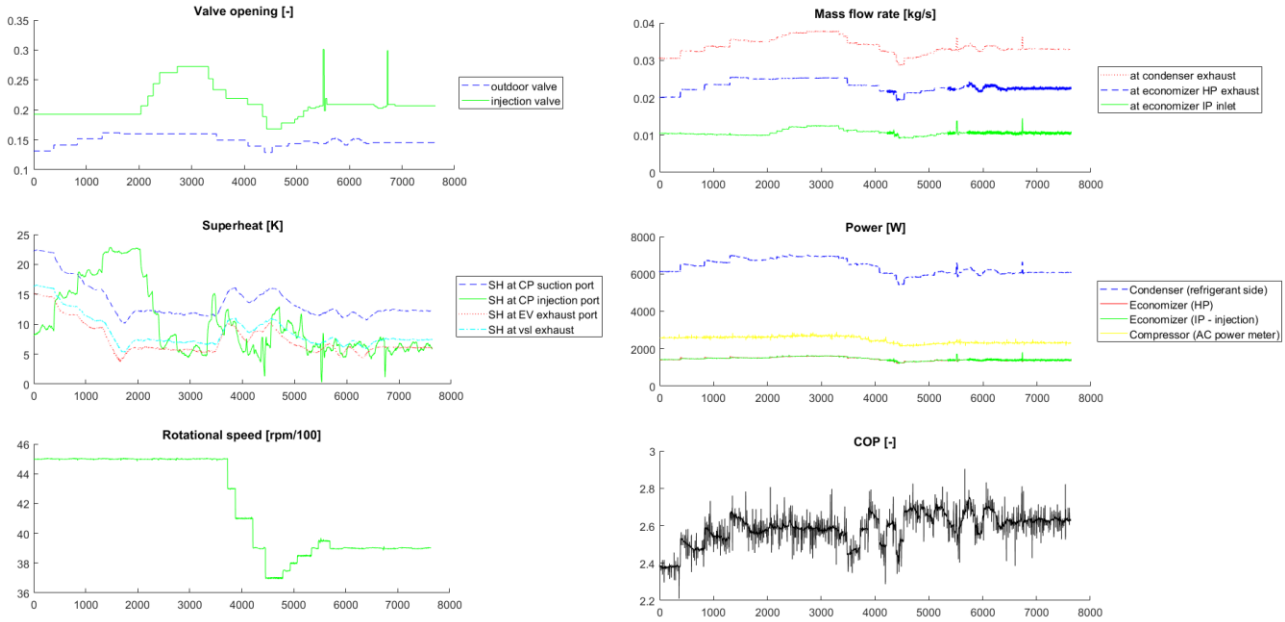

Figure 3: Experimental results for superheat analysis with speed decrease to maintain equal heating capacity as a function of time [s].

In Figure 3, the same test was carried out at 4500 RPM and for an outdoor temperature of 7°C. The water supply temperature was set to 55°C. However, a third phase (time ∈ [3800; 7500] seconds) was added in order to compare system performance for a constant heating capacity. It can be concluded that a better open loop control of both level of superheat helped to decrease the rotational speed by more than 10% and the discharge temperature by 12.5K and increase the COP from 2.38 to 2.63 at constant heating capacity.

Table 2 gives an overview of the COP, discharge temperature and heating capacity evolution at the beginning of the test, the end of phase I and end of phase II for different working conditions. First of all, for all working conditions, the COP and heating capacity can be increased by respectively around 10% and 15% while the discharge temperature is decreased if the superheat degrees are decreased from 15K to 5K for the suction superheat and 10K to 5K for the injection superheat. Moreover, the suction superheat has a major impact on the system COP and heating capacity while the injection superheat main impact is on the discharge temperature of the compressor. This impact is however important as decreasing this temperature can help to extend the operating envelope of the compressor.

Table 2: COP, discharge temperature and heating capacity variation at the beginning of each test, end of phase I and II for several working conditions.

N	T_{out}	T_{water}	COP			$\Delta\dot{Q}_{cd}$ [%]			T_{dis} [°C]		
rpm	°C	°C	t = 0s	I	II	t = 0s	I	II	t = 0s	I	II
3000	0	50	2.25	2.54	2.56	0	16.0	19.0	115	110	103
4500	0	50	2.24	2.50	2.55	0	14.5	19.4	120	112	106
6000	0	50	2.16	2.34	2.36	0	11.7	14.4	124	120	113
4500	7	55	2.38	2.57	2.58	0	11.7	14.4	118	113	106
6000	7	55	2.26	2.39	2.38	0	7.7	10.2	123	114	106

It is shown in this section that the control of the injection line superheat is coupled with the control of the suction superheat. In the following sections, a decoupled controller is presented in order to improve the control of the injection line superheat by decoupling it via a feedforward action.

3. MODELING AND CONTROL

In the first part of this section, the models used in order to develop and test an adapted controller that takes into account the coupling between the injection superheat and the OEEV opening are presented. The proposed controller is then tested in simulation for one operating point using the nonlinear dynamic model of the injection line. Due to the nonlinear behavior of the system, the proposed controller parameters should be scheduled in order to get a global adaptive controller that can be used under any operating conditions.

3.1 System decoupler

The controller is based on a decoupler as proposed by Åström *et al.* (2001). In fact, the superheat is usually controlled using a PID controller in refrigeration systems and the easiest way to take into account the coupling described in the previous section is the addition of a feedforward action (the decoupler) to the PID controller. In order to decouple the current system, a decoupler matrix *D(s)* is placed before the open loop process *G(s)* so that the resulting open loop transfer matrix *T(s)* is diagonal. In the particular case of the superheat control with the expansion valve opening, it was identified in section 2.2 that there was a coupling between the control of the OEEV and the injection superheat while there was no coupling between the suction superheat and the control of the IEEV. The process model and the decoupler matrix can thus be written as follow, where the outputs ΔSH and inputs ΔX are, respectively, the superheat and expansion valve opening variations.

$$\begin{pmatrix} y_1 \\ y_2 \end{pmatrix} = \boldsymbol{G}(s)\begin{pmatrix} u_1 \\ u_2 \end{pmatrix} \leftrightarrow \begin{pmatrix} \Delta SH_{su} \\ \Delta SH_{inj} \end{pmatrix} = \begin{pmatrix} G_{11}(s) & 0 \\ G_{21}(s) & G_{22}(s) \end{pmatrix}\begin{pmatrix} \Delta X_{oeev} \\ \Delta X_{ieev} \end{pmatrix} \quad (1)$$

$$\boldsymbol{D}(s) = \boldsymbol{G}^{-1}(s)\boldsymbol{T}(s) \leftrightarrow \boldsymbol{D}(s) = \frac{1}{G_{11}(s)G_{22}(s)}\begin{pmatrix} G_{22}(s)T_{11}(s) & 0 \\ -G_{21}(s)T_{11}(s) & G_{11}(s)T_{22}(s) \end{pmatrix} \quad (2)$$

If it is considered that the diagonal terms of $\boldsymbol{D(s)}$ are part of the PID controller and the non-diagonal terms of $\boldsymbol{D(s)}$ as a feedforward action, i.e. D_{11} and D_{22} are equal to one, the decoupler matrix becomes

$$\boldsymbol{D}(s) = \begin{pmatrix} 1 & 0 \\ -G_{21}(s)/G_{22}(s) & 1 \end{pmatrix} \quad (3)$$

It has to be noted that, as one of the non-diagonal terms of $\boldsymbol{G(s)}$ is equal to zero, the relative gain array matrix $\boldsymbol{\Lambda(G)}$ (RGA) (Bristol, 1966) is always equal to the identity matrix.

$$\boldsymbol{\Lambda}(G) \triangleq \mathbf{G} \times (\mathbf{G}^{-1})^T \tag{4}$$

In this case, a static decoupler is usually sufficient and the feedforward gain will be given by:

$$K_{ff} = D_{21}(0) = -G_{21}(0)/G_{22}(0) \tag{5}$$

In the two following sections, the application of this static decoupler will be tested on a particular operating point (presented in figure 3). Due to intrinsic non-linearity of the system, the PID and feedforward action gains should be identified and then scheduled.

3.2 Injection line models

In this section, the open loop model transfer functions, i.e. $G_{22}(s)$ and $G_{21}(s)$, are identified in order to calibrate the multivariable controller, i.e. the PID and feedforward action gains. Taking into account the responses showed in figures 2 and 3 for the injection superheat, a first order (FO) transfer function is the most suitable linear model for both terms. A global optimization algorithm is used to find the static gain and time constant of $G_{22}(s)$ and $G_{21}(s)$ by minimizing the root mean square of the output error using data from figure 3.

Moreover, a non-linear model of the injection line is developed in order to test first in simulation the proposed adapted controller. This model is presented in figure 4 along with the prediction results for the injection mass flow rate and superheat. It is developed in the Modelica language and is based on the ThermoCycle library (Quoilin, 2014) and CoolProp for the thermodynamic properties (Bell, 2014). The model and its components are described in detailed in Dechesne *et al.* (2017, 2018). The model takes as inputs the pressure and enthalpy at the suction port of the compressor, the condenser pressure, the compressor speed and both valves opening.

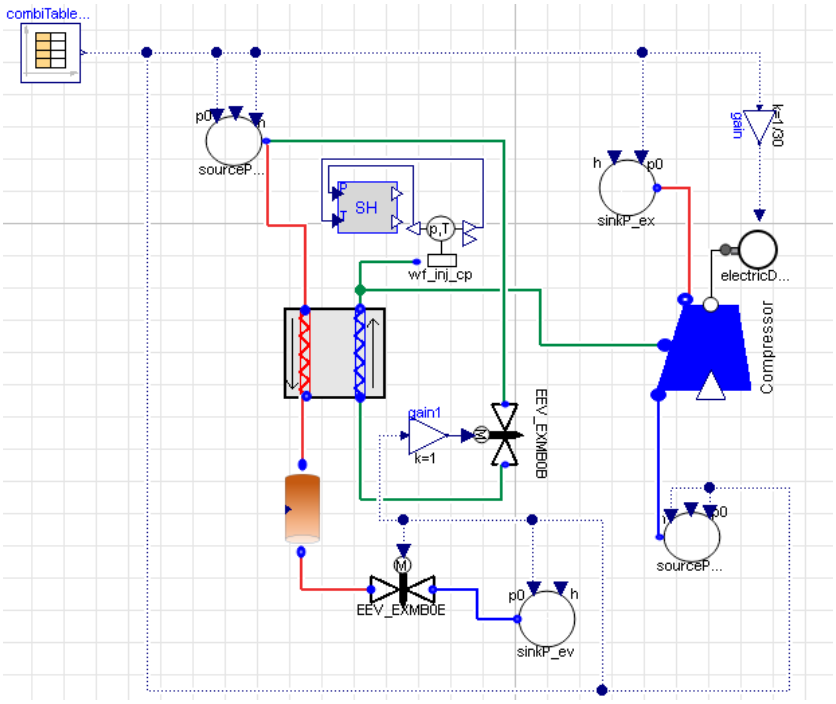

Figure 4: Dymola model.

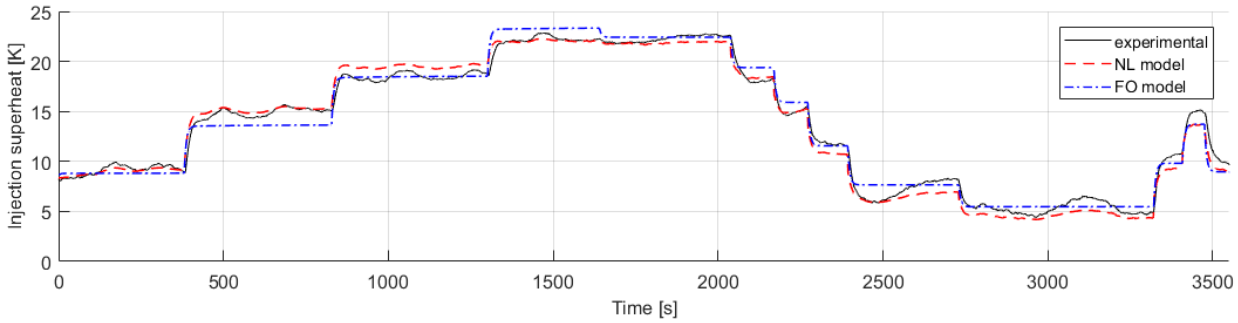

Figure 5: FO and non-linear model injection superheat prediction vs measurements.

It has to be noted that the prediction of the superheat is not easy as a small prediction error on the power or mass flow rate has a big impact on the superheat prediction due to the small thermal capacity of the fluid. The following conclusions can be drawn from figure 5:

- The non-linear Dymola model predicts accurately the dynamics of the system and can thus be used to test the new controller.
- The use of FO transfer functions for the injection superheat response is justified.

3.3 Adapted controller with decoupler

In this section, the addition of the decoupler in the PID controller of the system is tested on the validated non-linear model presented in Sec. 3.2. This controller is compared to the baseline SISO PID controller that is currently implemented on the system. PID controller gains are chosen using the PID-IMC (Internal Model Control) method for a first order process transfer function (Chien, 1990). The filter time constant T_m is set to half of the process time constant T, hence, the gains for a standard PI form are given by

$$K_c = \frac{T_{22}}{T_m K_{22}} = \frac{2}{K_{22}} \,\&\, T_i = T_{11} \tag{6}$$

The feedforward open loop transfer function is given by

$$K_{ff}(s) = -G_{21}(s)/G_{22}(s) = \frac{-K_{21}}{K_{22}} \frac{1 + T_{22}s}{1 + T_{21}s} \tag{7}$$

In the case of the static decoupler, it becomes:

$$K_{ff} = -G_{21}(0)/G_{22}(0) = -K_{21}/K_{22} \tag{8}$$

The new controller scheme is presented in figure 6 where

- The inputs u_1 and u_2 are respectively the OEEV and IEEV openings (X_{oeev} and X_{ieev});
- The output y_2 is the injection superheat SH_{inj};
- The output reference $y_{2,r}$ is the injection superheat set point.

Finally, the simulations results are given in figures 7 and 8 for four different controllers:

- A baseline PI controller;
- A PI controller with a static decoupler as the feedforward action;
- A PI controller with the same static decoupler that is delayed by a dead time T_{dt}. Hence, in this case, the feedforward action is delayed by a dead time T_{dt};
- A PI controller with a dynamic decoupler. In this case, the transfer function described in equation (7) is used without taking s=0.

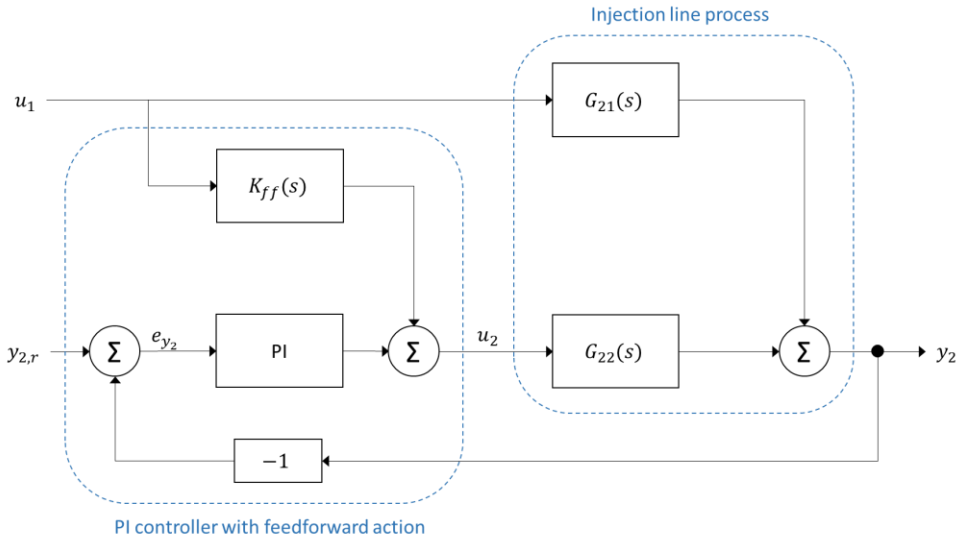

Figure 6: PI controller for the injection line with feedforward action as a decoupler.

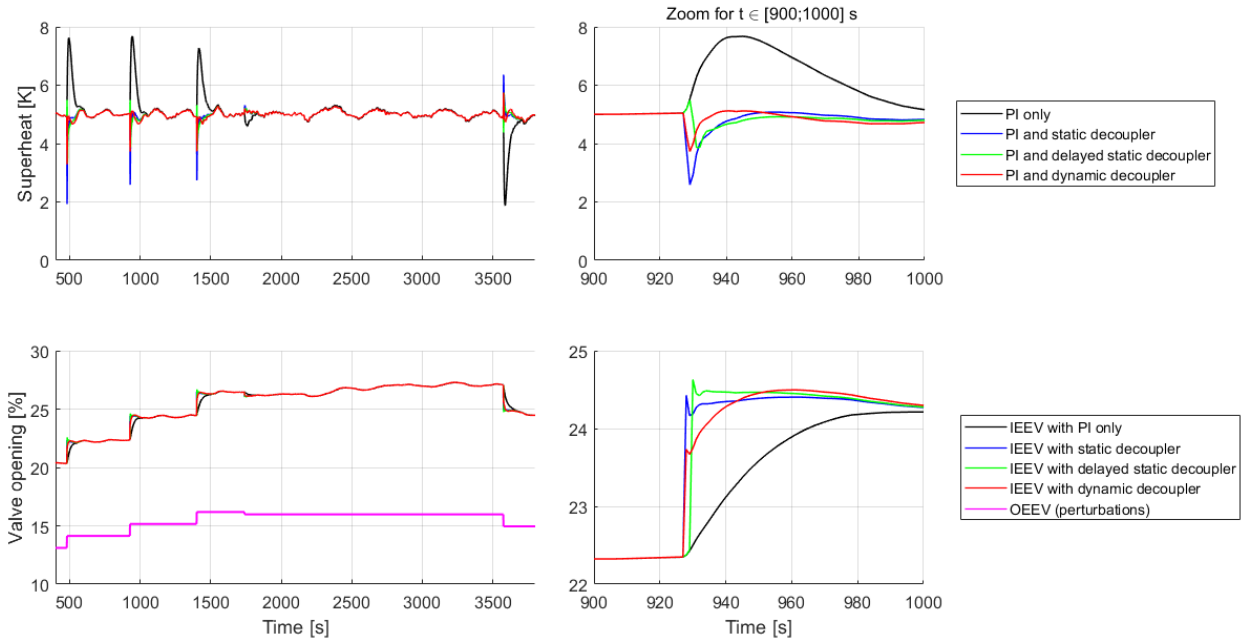

Figure 7: Comparison of four controllers using experimental data presented in figure 3.

It can be seen in figure 7 that, for a superheat set point of 5K, the three decoupler based controllers helps to decrease more rapidly than the PI control the unexpected variation of the injection superheat with the opening of the OEEV. The valve opening response shows clearly that the IEEV reacts faster to the OEEV opening variation when the decoupler is used. However, especially for the static decoupler result (blue line), it can be seen that some overcompensation can occur and the superheat drops instead of increasing when the OEEV opening increases. More precisely, the compensation happens too fast, which causes the superheat to drop before the system stabilizes to the set-point. This observation is the motivation of the test of the second controller (green line) which is a static decoupler with a dead-time T_{dt} of 2 seconds (chosen arbitrary) was investigated. This dead-time helps to decrease the overcompensation by letting the system reacts first during the dead-time before the feedforward action is taken into account. The zoom diagrams in figure 7 shows that this dead-time helps to decrease this over-compensation. Finally, the dynamic decoupler shows the best performances with even less over-compensation and a shorter stabilization time.

This is clearly seen on the zoomed diagram of the IEEV opening where the dynamic decoupler helps to decrease the feedforward reaction in the first moments after the change of the OEEV opening.

Finally, in figure 8, a multisine signal has been added to the OEEV opening data from figure 3 starting after 50 seconds in order to increase the disturbance. A constant superheat set-point for all controllers has been calculated in order to maintain, at any time of the simulation, an injection superheat above 0.5K. It can be seen that the controller with the dynamic decoupler performs the best with an injection superheat set-point that can be decreased from 7.2 to 2.7 K. The increase of the injection mass flow rate and the decrease of the compressor discharge temperature mean values are also presented in table 3. Based on the simulation, the gain in term of injection mass flow rate increase is rather small and the same conclusion can be drawn for the discharge temperature. However, the decoupler also helps to maintain the system in steadier operation as the standard deviation around the average value is decreased which can be interesting to increase the compressor lifetime.

These results are of course highly dependent on the perturbation type and amplitude and thus the proposed controllers should be tested on the test bench under real-life operating conditions. However, this study clearly shows that the controller with a decoupler performs better in term of injection superheat control than pure conventional PI.

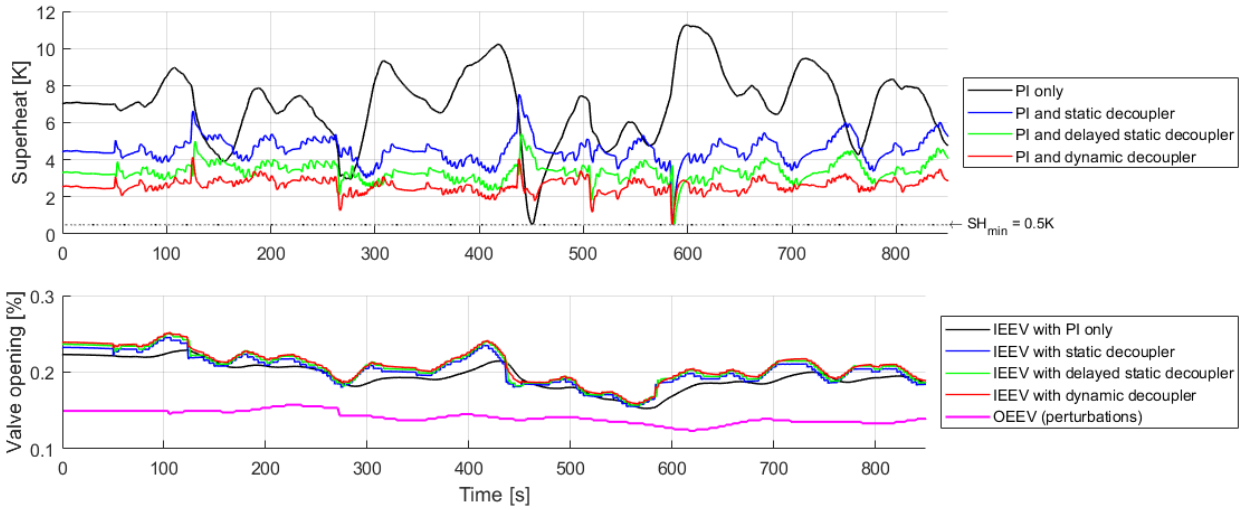

Figure 8: Superheat evolution comparison for the four controllers with multisine excitations.

Table 3: Injection line controller results in the presence of disturbance on u_1 (OEEV opening)

Controller	**SH Setpoint**	**SH Average**	**SH Standard deviation**	**Injection mass flow rate increase**	**Average discharge temperature**
	K	K	K	%	K
PI	7.2	7.0	1.9	-	109.0
PI with static decoupler	4.6	4.5	0.7	2.0	107.8
PI with delayed static decoupler	3.4	3.4	0.5	3.0	107.2
PI with dynamic decoupler	2.7	2.6	0.4	3.6	106.8

4. CONCLUSIONS AND FUTURE WORK

In this paper, the impact of the superheat control on the heat pump performance is presented. It was first shown that the four-way valve has a significant impact on the level of superheat at the suction port of the compressor. In fact, this component behaves as a small heat exchanger between the high pressure hot gases and the colder, low pressure gases entering the compressor. Moreover, the coupling of the superheat control for both the suction and injection superheat was presented. This exhibits the need of advanced control for this kind of system, as a simple SISO PID controller is not optimal. Furthermore, it was shown for different working conditions that the level of superheat has a significant impact on the system performance. The COP and heating capacity can be increased by about 10 and 15% while the discharge temperature is decreased by more than 10K if the superheat level is decreased from 15 to 5K.

In the second part of the paper, the addition of a feedforward action to the control of the injection expansion valve was proposed in order to take into account the coupling with the control of the outdoor EEV. The proposed multivariable controllers were compared to a baseline PI controller on one operating point using a non-linear model developed in Dymola. Three multivariable controllers were tested and the dynamic decoupler showed the best performances. It was shown that it outperformed the basic PI controller in term of superheat stability and, in practice, this allowed the superheat set-point to be decreased by 4.5K compared to the PI controller.

As it was mentioned in section 3, the gains of the proposed controller have to be adapted depending on the working conditions. The FO transfer functions have thus to be calculated for different operating conditions and an interpolation method has to be defined for gain scheduling. A real implementation and an experimental validation of the decoupler controller could also be interesting in order to prove the robustness of the proposed methodology. Moreover, the control of the suction line can be improved by taking into account the effects of the vapor split line and the four-way that were described in section 2.2.

REFERENCES

Åström, K. J., Johansson, K. H., & Wang, Q. G. (2002). Design of decoupled PI controllers for two-by-two systems. *IEE Proceedings-Control Theory and Applications*, *149*(1), 74-81.

Bell, I. H., Wronski, J., Quoilin, S., & Lemort, V. (2014). Pure and pseudo-pure fluid thermophysical property evaluation and the open-source thermophysical property library CoolProp. *Industrial & engineering chemistry research*, *53*(6), 2498-2508.

Bristol, E. (1966). On a new measure of interaction for multivariable process control. *IEEE transactions on automatic control*, *11*(1), 133-134.

Chien, I. L. (1990). Consider IMC tuning to improve controller performance. *Chem. Eng. Prog. 86*, 33-41.

Dechesne, B., Gendebien, S., Lemort, V., & Bertagnolio, S. (2017). Comparison of a dynamic model and experimental results of a residential heat pump with vapor injection and variable speed scroll compressor. In *Proceedings of ECOS 2017*.

Dechesne, B. & Lemort, V. (2018). Modeling and experimental results of a residential heat pump with vapor injection and variable speed scroll compressor. In *Proceedings of REHVA Annual Meeting 2018*.

Heo, J., Jeong, M. W., Baek, C., & Kim, Y. (2011). Comparison of the heating performance of air-source heat pumps using various types of refrigerant injection. *International Journal of Refrigeration*, *34*(2), 444-453.

Park, C., Lee, H., Hwang, Y., & Radermacher, R. (2015). Recent advances in vapor compression cycle technologies. *International Journal of Refrigeration*, *60*, 118-134.

Quoilin, S., Desideri, A., Wronski, J., Bell, I., & Lemort, V. (2014). ThermoCycle: A Modelica library for the simulation of thermodynamic systems. In *Proceedings of the 10th International Modelica Conference; Lund; Sweden* (No. 96, pp. 683-692).

Xu, X., Hwang, Y., & Radermacher, R. (2011). Refrigerant injection for heat pumping/air conditioning systems: literature review and challenges discussions. *International Journal of Refrigeration*, *34*(2), 402-415.